Detergent organisation in crystals of monomeric outer membrane phospholipase A

Snijder, HJ; Timmins, PA; Kalk, KH; Dijkstra, BW

Published in:
Journal of Structural Biology

DOI:
10.1016/S1047-8477(02)00579-8

Publication date:
2003

ACADEMIC PRESS

Available online at www.sciencedirect.com

SCIENCE DIRECT®

Journal of Structural Biology 141 (2003) 122–131

Journal of Structural Biology

www.elsevier.com/locate/yjsbi

Detergent organisation in crystals of monomeric outer membrane phospholipase A

H.J. Snijder,[1] P.A. Timmins,[2] K.H. Kalk, and B.W. Dijkstra*

Laboratory of Biophysical Chemistry, BIOSON Research Institute and Groningen Biomolecular Sciences and Biotechnology Institute, University of Groningen, Nijenborgh 4, NL-9747 AG Groningen, The Netherlands

Received 5 August 2002, and in revised form 17 October 2002

Abstract

The structure of the detergent in crystals of outer membrane phospholipase A (OMPLA) has been determined using neutron diffraction contrast variation. Large crystals were soaked in stabilising solutions, each containing a different H_2O/D_2O contrast. From the neutron diffraction at five contrasts, the 12 Å resolution structure of the detergent micelle around the protein molecule was determined. The hydrophobic β-barrel surfaces of the protein molecules are covered by rings of detergent. These detergent belts are fused to neighbouring detergent rings forming a continuous three-dimensional network throughout the crystal. The thickness of the detergent layer around the protein varies from 7–20 Å. The enzyme's active site is positioned just outside the hydrophobic detergent zone and is thus in a proper location to catalyse the hydrolysis of phospholipids in a natural membrane. Although the dimerisation face of OMPLA is covered with detergent, the detergent density is weak near the exposed polar patch, suggesting that burying this patch in the enzyme's dimer interface may be energetically favourable. Furthermore, these results indicate a crucial role for detergent coalescence during crystal formation and contribute to the understanding of membrane protein crystallisation.

Keywords: Contrast variation; Crystallisation; Detergent structure; Membrane proteins; Neutron diffraction; Outer membrane phospholipase

1. Introduction

The worldwide effort put into membrane protein research contrasts sharply with the number of membrane proteins whose structures have been determined to near-atomic resolution. This lack of structural information is at least partly related to difficulties with obtaining suitable crystals of membrane proteins. The amphiphilic nature of the protein's surface, with large hydrophobic and hydrophilic areas, generally requires detergent solubilisation. The detergent needs to be accommodated in the crystal lattice, but supplies few specific interactions that may lead to crystal contacts. Knowledge of the factors that govern their crystallisation may help to rationalise the quest for diffraction quality crystals of membrane proteins. In this respect, analyses of the packing of detergent and membrane proteins in the crystal may contribute to achieving this (Pebay-Peyroula et al., 1995; Penel et al., 1998; Roth et al., 1991, 1989). The structure of the detergent phase cannot be determined routinely using X-ray diffraction, owing to the fluidity of the detergent molecules and their low X-ray contrast. In contrast, neutron diffraction combined with H_2O/D_2O contrast variation (Roth, 1991) allows the study of the partially ordered detergent in crystals. Recently, noble gas soaking has also been exploited to successfully map the detergent in porin crystals by low-resolution X-ray diffraction (Sauer et al., 2002). Here, we have employed single crystal neutron diffraction to elucidate the organisation of the β-octylglucoside (β-OG)[3]

* Corresponding author. Fax: +31-(0)50-3634800.
E-mail address: b.w.dijkstra@chem.rug.nl (B.W. Dijkstra).
[1] Present address: Department of Chemistry and Bioscience, Chalmers University of Technology, P.O. Box 462, SE-485 30 Göteborg, Sweden.
[2] Large Scale Structures Group, Institute Laue-Langevin, 6 rue Horowitz, BP156, 38042 Grenoble, France.

[3] *Abbreviations used:* OMPLA, outer membrane phospholipase A; β-OG, 1-*O*-*n*-octyl-β-D-glucopyranoside; MPD, 2-methyl-2, 4-pentanediol.

1047-8477/02/$ - see front matter © 2002 Elsevier Science (USA). All rights reserved.
doi:10.1016/S1047-8477(02)00579-8

detergent phase in crystals of monomeric outer membrane phospholipase A (OMPLA) from *Escherichia coli* and have analysed xenon binding to OMPLA.

Outer membrane phospholipase A is an integral membrane phospholipase, which is present in many Gram-negative bacteria (reviewed in Snijder and Dijkstra, 2000). Its 3D-structure consists of a 12-stranded antiparallel β-barrel with a convex and a flat side. The active site residues are exposed on the exterior of the flat face of the β-barrel. The activity of the enzyme is regulated by reversible dimerisation (Dekker et al., 1997). Dimer interactions occur exclusively in the membrane-embedded parts of the flat side of the β-barrel, with polar residues embedded in an apolar environment forming the key interactions (Snijder et al., 1999). In monomeric OMPLA these polar residues are exposed to the hydrophobic interior of the membrane. Since the detergent is thought to mimic the natural membrane, elucidation of the detergent organisation can give clues on the interaction of these exposed polar residues with the lipid.

2. Methods

2.1. Crystallisation and soaking

Crystals of monomeric OMPLA were grown by mixing protein solution (30 mg/ml OMPLA, 10 mM succinate buffer, pH 6.5, 1.5% (w/v) 1-*O*-*n*-octyl-β-D-glucopyranoside, 1 mM NaN_3) in a 3:2 ratio with a reservoir solution containing 25–29% (v/v) 2-methyl-2,4-pentanediol (MPD), 1 mM $CaCl_2$, and 0.1 M bis-Tris, pH 5.9–6.0 (Blaauw et al., 1995). Rounds of macro seeding were necessary to obtain crystals of sufficient dimensions (typically $1.3 \times 0.4 \times 0.2\,mm^3$). Crystals were soaked for at least 2 weeks in stabilising mother liquors (29% (v/v) MPD, 1 mM $CaCl_2$, 0.1 M bis-Tris, pH 5.9–6.0, and 1.5% (w/v) β-OG) with different D_2O contents. The highest contrast which could be attained was with a mother liquor in which the solvent phase contains 71% (v/v) D_2O and 29% (v/v) MPD. This has a scattering length density which is calculated to be 0.445×10^{-15} m/A^3 equivalent to a D_2O/H_2O solvent of 74% v/v D_2O assuming that the MPD is uniformly distributed throughout the aqueous phase.

2.2. Data collection and data processing

Diffraction experiments were performed on the DB21 4-circle diffractometer at the Institut Laue-Langevin (Grenoble, France) at a fixed neutron wavelength of 7.53 Å. The instrument was equipped with a two-dimensional position-sensitive scintillation-detector of the Anger camera type (Roche et al., 1985). The crystal-detector distance was 250 mm and the camera had a 2θ swing out of 14° or 20°, which gives a highest attainable resolution of approximately 10 Å. Data were collected with exposure times of 15–20 min per 0.2° oscillations. For complete sampling of the reciprocal space, multiple crystal orientations were used, while for the 14.5% D_2O data were collected from two different crystals. Neutron transmission experiments were used to scale the contrast of the MPD/water mixtures to that of pure water. Data were collected at five different D_2O solvent contents (0, 14.5, 33.0, 46.8, and 61.2%).

The crystal orientation matrix was determined using an interactive computer graphics approach using the programs Maindex (Penel and Legrand, 1997) and O (Jones et al., 1991). Data integration and reduction were done with a customised version of XDS (Kabsch, 1993). Data collection statistics are listed in Table 1. The completeness at higher resolution (13–10 Å) is relatively low due to detector geometry and data collection time limitations. Therefore, the effective resolution of the combined data is approximately 12 Å.

2.3. Data scaling and structure factor calculation

For the acentric reflections the diffraction intensities resulting from a contrast variation experiment show a quadratic relation with the contrast (D_2O content). For the centric reflections, which have their phases restricted, the structure factor amplitude shows a linear variation with the contrast. These relations were used to scale the five data sets together (Roth et al., 1984). In

Table 1
Neutron diffraction data statistics

	D_2O contrast				
	0.0%	14.5%	33.0%	46.8%	61.4%
Resolution (Å)	68–10.9	68–10.4	68–11.3	68–10.5	68–10.7
Observed reflections	324	812	187	484	316
Unique reflections	157	193	116	150	174
R_{sym}[a] (%)	5.1	12.2	3.3	3.0	4.9
Completeness (%)	74.1	86.9	67.0	75.0	86.1
$\langle I/\sigma I \rangle$	8.2	13.9	7.4	16.3	10.5

[a] R_{sym} defined as $\sum_{hkl} \sum_i |I_i(hkl) - \langle I(hkl) \rangle| / \sum_{hkl} \sum_i I_i(hkl) * 100\%$.

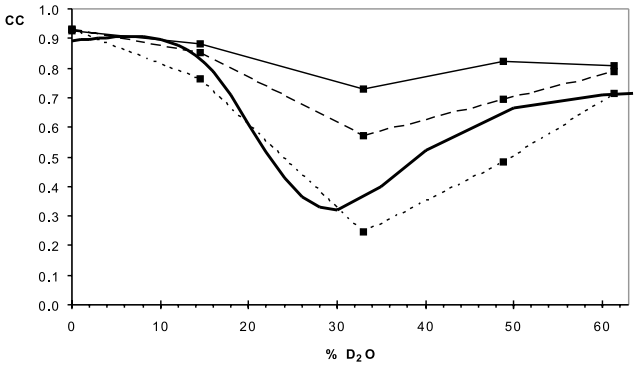

Fig. 1. Correlation between observed and calculated structure factor amplitudes as a function of D_2O concentration. The correlation between calculated structure factors from the protein model alone and the interpolated structure factor amplitudes is shown by the thick solid curve. The other three curves indicate the correlation of the observed structure factor amplitudes with those calculated from: the protein alone (short dashes), the protein and the first detergent model (long dashes), and the protein and the final detergent model (solid lines).

space group $P3_121$ reflections can be indexed using two equally valid axis definitions, which differ by a rotation of 60°. As for each data set this definition is made independently of other collected data sets, this leads to 16 different combinations for five data sets. The selection of a consistent choice of axis definition was done on the basis of the scaling *R*-factor. The most consistent choice resulted in the lowest *R*-factor (6.3%). Incorrect combinations gave *R*-factors in the range of 13–20%.

The contrast variation method supplies relative phase relationships between structure factors at different contrasts. Determination of absolute phases requires additional information. For this, we used the protein coordinates from the OMPLA monomer determined by X-ray crystallography as the partial starting model (Snijder et al., 1999). First, the contrast at which the detergent contributed least to the diffraction was determined by comparing the structure factor amplitudes obtained from the experimental data, with structure factors calculated from the protein model. The maximum correlation was found at 10% D_2O; in a finer systematic search the maximum correlation was found at 6% D_2O (Fig. 1), thus close to the match point of the hydrophobic tails of the detergent (1.8% D_2O). With this phase information centroid maps at any contrast can be calculated (Roth, 1987).

2.4. Modeling and refinement

At low resolution the contrast, which allows a molecule to be imaged, is the scattering length difference between the molecule and its (usually) aqueous environment. In pure D_2O/H_2O solution the scattering of protein is the same as that of a solution containing close to 40% D_2O/60% H_2O. That of hydrocarbon may be in the range 0–10% D_2O. In our case the surrounding solvent contains also 29% MPD as explained above. For this reason we calculated the scattering length density of each MPD/D_2O/H_2O mixture and related it to a D_2O/H_2O solvent of the same contrast. In the following the term x% D_2O is referred to as the contrast produced by a solvent with scattering length density the same as that of an x% D_2O/H_2O solvent. Initially centroid scattering length density maps at 10, 40, and 100% D_2O were calculated. The 10% map was used to create an envelope that defined the protein. A first model of the detergent was obtained from the 40% map, corresponding to the match point of the protein (Fig. 2). The most negative regions outside the protein envelope were modeled as hydrophobic detergent tails. The detergent volume fraction in the crystals is not known and a first estimate of about 7% was made by visual inspection of the 40% contrast map. Solvent regions were flattened and subsequently the density was smoothed by local pixel density averaging using a linearly decreasing weight and a cutoff radius of 8 Å. The modeled density was then transformed into pseudo-atoms. Scattering densities of half a hydrophobic β-OG tail were used as the scattering density of the pseudo-atoms. Phases were recalculated using structure factors from the protein model and the pseudo-atoms; the additional information allows calculation of the best estimate structure factors. Thus, structure factors were improved in an iterative process of map modeling and phase calculation. The quality of the model was monitored by an *R*-factor or correlation coefficient, which indicates the agreement between the calculated and the measured structure factors amplitudes at different contrasts.

Finally, the detergent volume in the crystals was estimated by monitoring the correlation between model

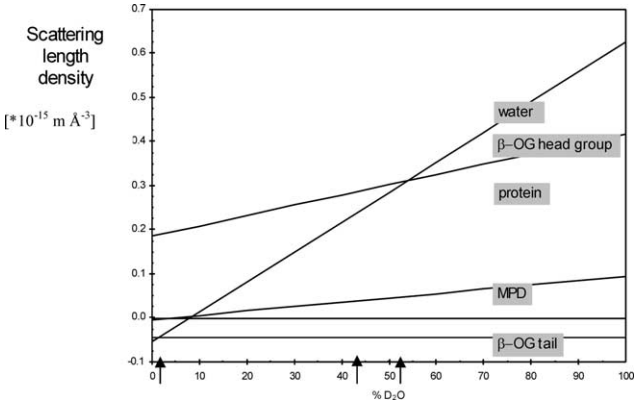

Fig. 2. Scattering-length densities as a function of D_2O concentration are plotted for water, a typical protein, tail region of β-OG, head group of β-OG, and 2-methyl-2,4-pentanediol (MPD). The match points for the protein and the detergent are marked by arrows on the abscissa. The volumes used in the calculations are 212.9, 180.3, and 236.7 Å^3, for MPD, β-OG head groups, and β-OG tails, respectively (Timmins et al., 1994).

and measurements as a function of the modeled detergent volume. A broad optimum was found between 8 and 12% volume of the unit cell. Independently, the detergent was modeled in the 100% contrast map, where both detergent and protein have negative contrast with respect to the solvent. Using a detergent volume of 10%, modeling converged in three cycles and produced similar neutron maps. The scattering density maps at 40% contrast calculated for both models had a correlation coefficient of 0.9. Finally, both maps were averaged in real space to produce the final model density.

2.5. Xenon derivative

A xenon derivative was obtained by mounting an OMPLA crystal (size approximately $0.5 \times 0.2 \times 0.1\,mm^3$) in a short quartz capillary and applying 1.3×10^6 Pa of xenon pressure. The crystal was equilibrated for 1 h prior to data collection. During data collection the pressure gradually decreased to 1.0×10^6 Pa. Data were collected in house at ambient temperature (Mac Science DIP2030, Nonius FR591 rotating anode generator, CuKα radiation) and processed with DENZO and SCALEPACK (Otwinowski and Minor, 1997). Intensities were reduced to structure factor amplitudes using the program TRUNCATE from the CCP4 package (Collaborative Computational Project Number 4, 1994). Details of the data collection are given in Table 2. Difference density calculation was based on the native crystal structure of OMPLA (Snijder et al., 1999) stripped of its detergent and water molecules. This model was refined as a rigid body against native data collected at room temperature (Mac Science DIP2020 detector, Nonius FR591 rotating anode generator, CuKα radiation) using refinement protocols as implemented in XPLOR (Brünger, 1992). Difference density (Fig. 5) and anomalous difference maps were calculated with programs from the CCP4 package and were analysed with MAPMAN (Kleywegt and Jones, 1996). A low-resolution image of the xenon sites (70–10 Å) was made using the procedure described by Sauer et al. (2002). Xenon atoms were assigned in the difference density using a 3.5σ cutoff. However, some sites were buried in the protein interior or were solvent-exposed and clearly inaccessible to detergent. These sites were excluded from further calculations. The remaining atoms were given a *B*-factor of 50 A^2 and an occupancy depending on the peak height in the difference map. A back Fourier transformation yielded a calculated low-resolution xenon map.

3. Results and discussion

3.1. Phasing and model building

Fig. 1 shows that at 6% D_2O the protein contributes predominantly to the scattering, while the contribution of the detergent is minimal. Thus, the calculated structure factors from the protein model alone are closest to those determined experimentally when the scattering by the detergent is matched out. The match point of the detergent phase is close to that of the regions of the hydrophobic tails of the detergent. This indicates that the hydrophobic detergent regions dominate the scattering by the detergent (Fig. 2, the match point of the detergent tail is at 1.8% D_2O; the β-OG head group is matched at 52% D_2O (Timmins et al., 1994)).

Five cycles of modeling and phasing resulted in the final refined β-OG model. The scattering density of the detergent regions was assumed to correspond to that of the tail rather than the whole β-OG model because the correlation between observed and calculated structure factors was higher. Fig. 1 illustrates the evolution of the correlation between calculated and observed structure factor amplitudes in the course of the refinement. The correlation coefficient at 0% D_2O hardly changes during the refinement, owing to the small contribution of the detergent to the scattering at this contrast. At all other contrasts the correlation coefficient clearly increases. The volume fraction of the detergent in the crystals can be estimated from a systematic search for maximum correlation between calculated and observed structure factor amplitudes. The best agreement corresponded to a detergent fraction of 8–12%, which amounts to 31–46 β-OG molecules per enzyme monomer. The detergent was modeled in an independent way in 100% D_2O

Table 2
X-ray data collection statistics

Data set	Low resolution room temperature	Xenon soak room temperature
Space group	$P3_121$	$P3_121$
Cell dimensions	$a, b = 79.6$ Å	$a, b = 79.6$ Å
	$c = 102.5$ Å	$c = 103.1$ Å
Observed reflections	32494	19831
Unique reflections	5984	3565
Resolution	57.2–3.25 Å (3.37–3.25 Å)	20.0–3.9 Å (4.1–3.9 Å)
Completeness	95.5% (97.8%)	97.0% (97.5%)
R_{sym}[a]	7.0% (27.3%)	5.4% (11.1%)
$\langle I/\sigma \rangle$	19.9 (6.4)	17.5 (9.5)

[a] R_{sym} defined as $\sum_{hkl} \sum_i |I_i(hkl) - \langle I(hkl) \rangle| / \sum_{hkl} \sum_i I_i(hkl) * 100\%$.

contrast maps, which resulted in a similar detergent structure and a comparable optimum in the modeled volume fraction.

3.2. Detergent structure

Figs. 3 and 4 show the neutron scattering density map at 40% D_2O where the protein is matched out while the hydrophobic detergent tails have negative contrast. The detergent forms a band that encircles the protein and covers the exposed hydrophobic outer surface of the β-barrel. At the crystallographic twofold axis two such detergent rings coalesce. These double rings are intimately interconnected along the crystallographic 3_1 screw axis, thus forming a continuous network of detergent that extends throughout the whole crystal (Figs. 3a, 4c, and d).

The thickness of the detergent ring parallel to the protein barrel varies considerably with regions as thin as 7–8 Å. These thin regions originate from the exclusion of detergent due to direct hydrophobic crystal contacts along the 3_1 screw axis (Fig. 3b). At the β-barrel surfaces not involved in hydrophobic crystal contacts the detergent forms a band of 15–20 Å, slightly smaller than the thickness of the hydrophobic region in a typical lipid bilayer (Lewis and Engelman, 1983). At the convex side of the β-barrel two rings of aromatic residues delimit the modeled detergent density (Fig. 4a), similar to the rings observed in the detergent–protein structure of OmpF (Pebay-Peyroula et al., 1995; Penel et al., 1998) and the general porin from *Rhodobacter capsulatus* (Penel, 1997). The aromatic rings fulfill a role in delimiting the detergent phase. The opposite side of the OMPLA β-barrel, which is the functional dimerisation interface, shows a large disc-like detergent region that fills the space between the twofold related molecules. The covering of the dimerisation face by detergent corroborates that OMPLA may be accommodated in the membrane as a monomeric unit. The detergent density is particularly weak near the exposed polar patch on the dimerisation interface (shown by arrows in Figs. 3a–c) indicating that burying this patch in the enzyme dimer may be favourable.

3.3. Individual detergent molecules

The resolution of the neutron diffraction data prohibits assignment of individual detergent molecules, but

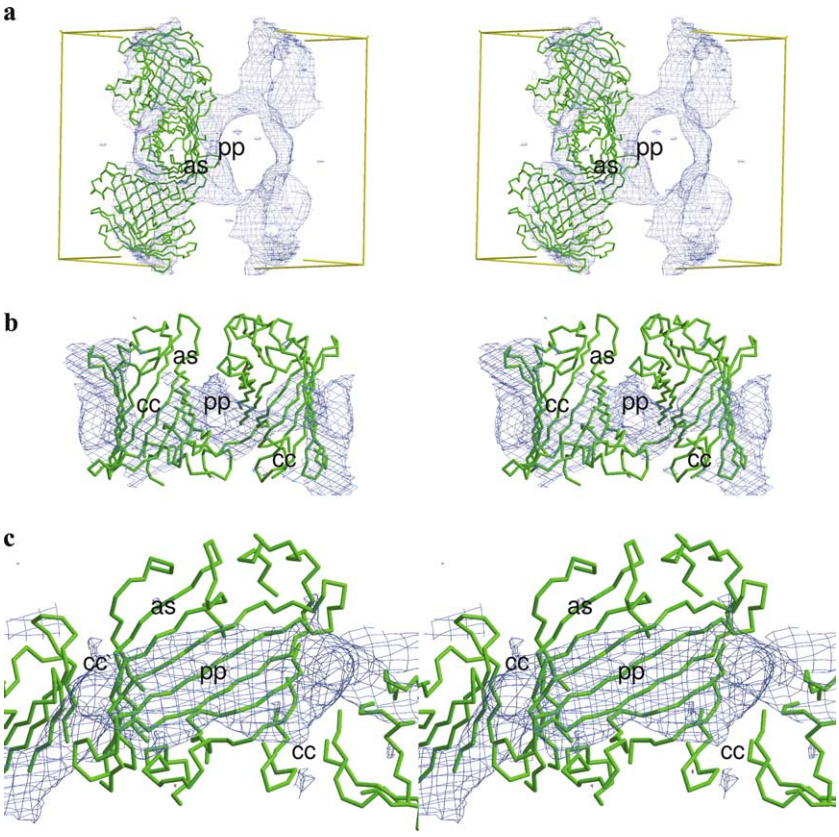

Fig. 3. Stereo diagrams showing the detergent organisation in OMPLA crystals. (a) View of 3_1-related OMPLA monomers. (b) View of the twofold related molecules. (c) View toward the dimerisation face of one OMPLA monomer. The contouring in all figures is such that a volume of 10% of the unit cell is enclosed. The active site of the enzyme is labeled with "as." The label "pp" highlights the thin detergent density near the polar patch on the dimerisation interface. The location of the hydrophobic crystal contacts is indicated by "cc."

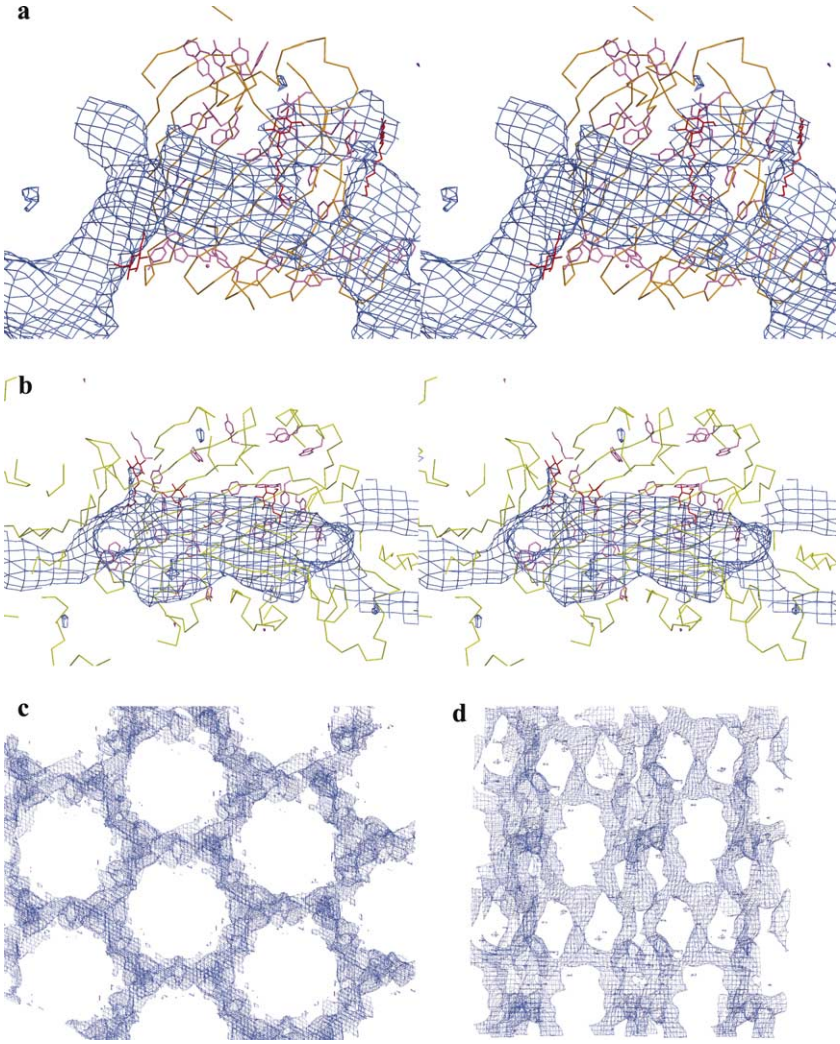

Fig. 4. Details and overview of the detergent structure. (a) View of the convex β-barrel surface showing two lines of aromatic residues that delimit the detergent phase. The individual detergent molecules that were identified in the high-resolution X-ray structure (Snijder et al., 1999) are depicted in stick representation in red. (b) Detergent structure at the flat side of the β-barrel shows individual detergent molecules stacked on aromatic residues (violet). (c and d) Two perpendicular orientations of the neutron map show that the detergent forms a continuous network that extends throughout the whole crystal.

in the 2.1 Å resolution X-ray structure two ordered detergent molecules could be modeled. Additionally three electron density features were interpreted as β-OG head groups with partly ordered tails (Snijder et al., 1999). The two complete detergent tails are found in the crevices created by packing two monomers together and fall within the detergent density in the neutron diffraction map. The detergent head groups are found at the periphery of the density and are mostly stacked on aromatic residues.

3.4. Comparison with other detergent–protein complexes

The detergent organisation in membrane protein crystals has also been determined for the photosynthetic reaction centres from *Rhodopseudomonas viridis* (Roth et al., 1989) and *Rhodobacter sphaeroides* (Roth et al., 1991), for two crystal forms of OmpF (Pebay-Peyroula et al., 1995; Penel et al., 1998) and for the general porin from *Rhodobacter capsulatus* (Penel, 1997). The detergent organisation in the crystals of the two reaction centres is pseudo-identical (Roth et al., 1991), but the detergent structures between the other crystals share only few and general similarities. The detergent phase covers the most hydrophobic membrane-spanning protein regions and displays both positive and negative surface curvature. Furthermore, in all examples detergent–detergent interactions are present that are crucial for crystal packing.

The detergent structures are remarkably diverse. The tetragonal crystal form of OmpF shows two independent lattices of porin trimers with undisturbed detergent belts surrounding each trimer. These lattices only interact via detergent head group/head group contacts

(Pebay-Peyroula et al., 1995). The trigonal form of OmpF is exceptionally different and shows layers of trimers. Within these layers the detergent has formed small distinct domains delimited by hydrophobic protein–protein crystal contacts (Penel et al., 1998). In both crystal forms of OmpF the detergent phase is discontinuous. In contrast, the reaction centres have a detergent phase that runs in chains throughout the crystals. The chains are formed from interconnected undisturbed detergent belts. In *Rhodobacter capsulatus* porin the detergent forms a continuous phase in two dimensions. The crystal consists of stacked layers of porin trimers; within these layers the detergent has formed one interconnected phase surrounding all trimers. However, only in the OMPLA crystals the detergent forms a fully continuous interconnected three-dimensional network.

3.5. Crystal packing and crystal growth

Membrane protein crystals are traditionally classed into two categories (Michel, 1983). Type I crystals consist of stacked layers of protein molecules. The crystals are held together by hydrophobic interactions in the plane of the layers (resembling 2D crystals), whereas polar contacts mediate interlayer interactions. Type II crystals have lattice contacts which involve only the polar regions of the membrane proteins. The hydrophobic regions are solvated by detergent micelles and direct hydrophobic interactions are absent. The packing of OMPLA molecules in the crystal does not obey either of the two types of membrane protein crystals. Here, a third crystal type (type III) is observed which consists of an intricate three-dimensional lattice formed by both hydrophobic and polar contacts.

The continuous detergent network and the hydrophobic crystal contacts suggest that during crystallisation OMPLA molecules approach each other closely and that merging of their detergent belts occurs. The formation of polar crystal contacts might drive crystallisation and induce merging of micelles after which detergent molecules could be expelled to allow hydrophobic crystal contacts. However, polar crystal contacts occur only between the molecules that are related by twofold rotational symmetry while along the 3_1-screw axis hydrophobic interactions occur. The polar contacts cannot drive fusion of micelles along the 3_1-screw axis, which suggests that the detergent belts themselves have a tendency to coalesce.

It is tempting to hypothesize that the coalescence of the detergent may be brought about by the precipitant 2-methyl-2, 4-pentanediol, which has been shown to act as an amphiphile (Kita et al., 1994) and which has a marked nonpolar character (Pittz and Bello, 1971). Moderate amounts of organic amphiphiles have been shown to be advantageous for membrane protein crystallisation, and their beneficial effect was attributed to increased micellar fluidity and deformability and decreased micellar size (Garavito et al., 1986; Marone et al., 1999; Michel, 1982, 1983; Papiz et al., 1989; Timmins et al., 1991). In higher concentrations (typical 20–25%) small amphiphiles even can induce a phase transition (Becher and Trifiletti, 1973). The high concentrations of MPD in the case of OMPLA may influence detergent micelles in a similar manner; a nonmicellar phase could explain the interconnected detergent network in the crystals and the availability of hydrophobic protein surfaces for crystal contacts.

This hypothesis is supported by the reports of the crystallisation and structure elucidation of OmpA (Pautsch and Schulz, 1998; Pautsch et al., 1999), OmpT (Vandeputte-Rutten et al., 2001), and OmpX (Vogt and Schulz, 1999). These membrane proteins form also type III membrane protein crystals and all are crystallised in the presence of large amounts of organic solvents. α-Helical membrane proteins can also form type III crystals, e.g., bacteriorhodopsin (Essen et al., 1998), cytochrome *c* oxidase (Iwata et al., 1995), and rhodopsin (Palczewski et al., 2000) form such crystals. The former two are crystallised with large amounts of organic solvents, whereas rhodopsin is crystallised using heptanetriol as additive. Thus, type III membrane protein crystals appear to be fairly general and organic amphiphiles may facilitate such a packing arrangement.

3.6. Xenon soaking

A crystal of OMPLA was subjected to pressurised xenon gas ($1.3–1.0 \times 10^6$ Pa) during data collection. The difference Fourier map between xenon-soaked and native crystals is shown in Fig. 5. The map shows one strong xenon site, which is the only site that is confirmed by the anomalous signal (not shown). This site is located in the β-barrel's interior, where a remarkably polar binding pocket is formed by the side chains of residues Glu117, Asn141, Arg157, Phe159, Lys174, and Trp176. Various sites with a lower occupancy are located in and around the β-barrel. The strongest of these minor sites are found on the hydrophobic exterior of the β-barrel. Xenon binds here in pockets formed by four hydrophobic side chains surrounding small surface depressions between two β-strands (Fig. 5b).

From the xenon sites a back-Fourier was calculated as described by Sauer et al. (2002). The calculated xenon-map (not shown) resembles to some extent the neutron diffraction detergent map, in the sense that the largest density is associated with the hydrophobic barrel exterior. However, the xenon map is discontinuous and shows a strong feature in the extracellular loop region of OMPLA.

The inability of the xenon map to convincingly resemble the neutron detergent density may originate from

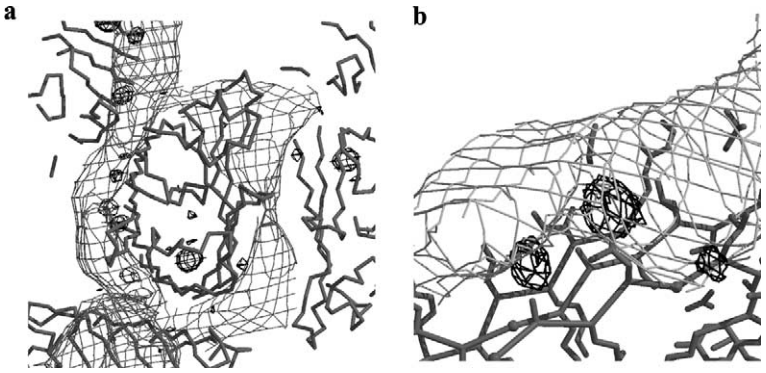

Fig. 5. $F_{obs\text{-}Xe}$–$F_{obs\text{-}Native}$ difference Fourier map from OMPLA after xenon exposure. (a) Overview of the xenon-binding sites, dark grey xenon difference density, light grey neutron diffraction detergent map. (b) Xenon binding at the hydrophobic β-barrel surface.

both practical and fundamental aspects. Nonisomorphism, reduced data quality, and strong X-ray absorption by pressurised xenon gas lead to increased noise levels in the difference map. Discrimination of sites with low xenon occupation from noise peaks is therefore difficult. Increase of xenon pressure may increase the occupancy at these sites.

A more fundamental issue arises because xenon can bind at sites different from the detergent (Fig. 5). As a consequence, before calculating a detergent image, some xenon sites must be rejected from the calculation based on rather subjective criteria. Another limitation of noble gas soaking to enhance contrast between solvent and detergent becomes evident when considering the X-ray contrast for the different components in the crystal (Table 3). Detergent molecules (here β-OG) have modestly positive contrast with respect to water, but the hydrocarbon part alone has negative contrast. Preferential accumulation of xenon in the hydrophobic part of the detergent micelle first decreases the contrast and only upon higher xenon concentrations increases it again. A simple calculation shows that more than 20% (v/v) of xenon should be present in a hydrocarbon region (n-C_8H_{18}) before the contrast starts to increase. Even if these high concentrations are within practical reach, such high xenon concentrations may introduce distortion of the detergent region. Moreover, the limited contrast will make it inherently difficult to resolve disordered or poorly occupied xenon atoms. Being dependent on high-resolution well-defined xenon-binding sites for the study of detergent localisation presents a serious limitation to this technique.

A more appealing approach is to exploit the natural X-ray contrast between the solvent and the hydrocarbon region of the detergent (Table 3) to model the disordered detergent region. This requires, however, good quality low-resolution data and a reliable method to determine low-resolution phases.

Table 3
Scattering density for neutron and X-ray diffraction[a]

	Å^3	10^{-15} cm Å^{-3}	e^- Å^{-3}
Water	30.0	−5.58	0.333
Average protein		19.20	0.440
OMPLA		20.82	0.449
MPD	203.6[b]	−0.39	0.324
29% (v/v) MPD		−4.09	0.331
β-OG	417.0[c]	5.53	0.384
β-OG head group	180.3[c]	18.61	0.527
β-OG tail	236.7[c]	−4.43	0.275
n-C_8H_{18}	269.5[b]	−5.25	0.245
n-C_8H_{18} with 0.53% (v/v) Xe[b,d,e]		−5.16	0.250
n-C_8H_{18} with 10.0% (v/v) Xe[b,d,e]		−3.69	0.334
n-C_8H_{18} with 20.0% (v/v) Xe[b,d,e]		−2.13	0.422

[a] Scattering lengths of the elements are taken from Neutron News, vol. 3. No. 3, pp. 29–37 (1992).

[b] Molecular volumes are calculated using densities ρ_{MPD} 0.964 g/ml and $\rho_{n\text{-}C8H18}$ 0.7025 g/ml from the Handbook of Chemistry and Physics, Weast and Astle (1983).

[c] Molecular volumes for the detergent are taken from Timmins et al. (1994).

[d] Solubility of xenon in water and n-C_8H_{18} are taken from Pollack (1981); Pollack and Himm (1982). A 0.53% (v/v) xenon is dissolved in n-C_8H_{18} at 1×10^5 Pa.

[e] A radius of 2.25 Å is used for Xe-atoms.

Acknowledgments

We thank R.L. Kingma, M.R. Egmond, and N. Dekker for their generous gift of protein material. This research was supported by the Netherlands Foundation for Chemical Research (C.W.) with financial aid from the Netherlands Organisation for Scientific Research (N.W.O.).

References

Becher, P., Trifiletti, S.E., 1973. Nonionic surface-active agents XIII. The effect of solvent on the thermodynamics of micellization. J. Colloid Interface Sci. 43, 485–490.

Blaauw, M., Dekker, N., Verheij, H.M., Kalk, K.H., Dijkstra, B.W., 1995. Crystallization and preliminary X-ray analysis of outer membrane phospholipase A from *Escherichia coli*. FEBS Lett. 373, 10–12.

Brünger, A.T., 1992. Free *R* value: a novel statistical quantity for assessing the accuracy of structures. Nature 355, 472–475.

Collaborative Computational Project Number 4, 1994. The CCP4 suite: programs for protein crystallography. Acta Crystallogr. D 50, 760–763.

Dekker, N., Tommassen, J., Lustig, A., Rosenbusch, J.P., Verheij, H.M., 1997. Dimerization regulates the enzymatic activity of *Escherichia coli* outer membrane phospholipase A. J. Biol. Chem. 272, 3179–3184.

Essen, L.O., Siegert, R., Lehmann, W.H., Oesterhelt, D., 1998. Lipid patches in membrane protein oligomers: crystal structure of the bacteriorhodopsin–lipid complex. Proc. Natl. Acad. Sci. USA 95, 11673–11678.

Garavito, R.M., Markovic-Housley, Z., Jenkins, J.A., 1986. The growth and characterization of membrane protein crystals. J. Crystal Growth 76, 701–709.

Iwata, S., Ostermeier, C., Bernd, L., Michel, H., 1995. Structure at 2.8 Å resolution of cytochrome *c* oxidase from *Paracoccus denitrificans*. Nature 376, 660–669.

Jones, T.A., Zou, J.-Y., Cowan, S.W., Kjeldgaard, M., 1991. Improved methods for building protein models in electron density maps and the location of errors in these models. Acta Crystallogr. A 47, 110–119.

Kabsch, W., 1993. Automatic processing of rotation diffraction data from crystals of initially unknown symmetry and cell constants. J. Appl. Crystallogr. 26, 795–800.

Kita, Y., Arakawa, T., Lin, T.-Y., Timasheff, S.N., 1994. Contribution of the surface free energy perturbation to protein–solvent interactions. Biochemistry 33, 15178–15189.

Kleywegt, G.J., Jones, T.A., 1996. xdlMAPMAN and xdlDATMAN—programs for reformatting, analysis and manipulation of biomolecular electron-density maps and reflection data sets. Acta Crystallogr. D 52, 826–828.

Lewis, B.A., Engelman, D.M., 1983. Lipid bilayer thickness varies linearly with acyl chain length in fluid phosphatidylcholine vesicles. J. Mol. Biol. 166, 211–217.

Marone, P.A., Thiyagarajan, P., Wagner, A.M., Tiede, D.M., 1999. Effect of detergent alkyl chain length on crystallization of a detergent-solubilized membrane protein: correlation of protein–detergent particle size and particle–particle interaction with crystallization of the photosynthetic reaction center from *Rhodobacter sphaeroides*. J. Crystal Growth 207, 214–225.

Michel, H., 1982. Three-dimensional crystals of a membrane protein complex. The photosynthetic reaction centre from *Rhodopseudomonas viridis*. J. Mol. Biol. 158, 567–572.

Michel, H., 1983. Crystallization of membrane proteins. Trends Biochem. Sci. 8, 56–59.

Otwinowski, Z., Minor, W., 1997. Processing of X-ray diffraction data collected in oscillation mode. Methods Enzymol. 276, 307–326.

Palczewski, K., Kumasaka, T., Hori, T., Behnke, C.A., Motoshima, H., Fox, B.A., Le Trong, I., Teller, D.C., Okada, T., Stenkamp, R.E., Yamamoto, M., Miyano, M., 2000. Crystal structure of rhodopsin: a G protein-coupled receptor. Science 289, 739–745.

Papiz, M.Z., Hawthornthwaite, A.M., Cogdell, R.J., Woolley, K.J., Wightman, P.A., Ferguson, L.A., Lindsay, J.G., 1989. Crystallization and characterization of two crystal forms of the B800–850 light-harvesting complex from *Rhodopseudomonas acidophila* strain 10050. J. Mol. Biol. 209, 833–835.

Pautsch, A., Schulz, G.E., 1998. Structure of the outer membrane protein A transmembrane domain. Nat. Struct. Biol. 5, 1013–1017.

Pautsch, A., Vogt, J., Model, K., Siebold, C., Schulz, G.E., 1999. Strategy for membrane protein crystallization exemplified with OmpA and OmpX. Proteins 34, 167–172.

Pebay-Peyroula, E., Garavito, R.M., Rosenbusch, J.P., Zulauf, M., Timmins, P.A., 1995. Detergent structure in tetragonal crystals of OmpF porin. Structure 3, 1051–1059.

Penel, S., 1997. Organisation du détergent dans les cristaux de protéines membranaires: analyse des cristaux des porines de *Rhodobacter capsulatus* et de *Escherichia coli*. Université Joseph Fourier.

Penel, S., Legrand, J.F., 1997. MAINDEX, Manual indexation for area-detector crystallographic data. J. Appl. Crystallogr. 30, 206.

Penel, S., Pebay-Peyroula, E., Rosenbusch, J., Rummel, G., Schirmer, T., Timmins, P.A., 1998. Detergent binding in trigonal crystals of OmpF porin from *Escherichia coli*. Biochimie 80, 543–551.

Pittz, E.P., Bello, J., 1971. Studies on bovine pancreatic ribonuclease A and model compounds in aqueous 2-methyl-2,4-pentanediol. Arch. Biochem. Biophys. 146, 513–524.

Pollack, G.L., 1981. Atomic test of the Stokes–Einstein law: diffusion and solubility of Xe. Phys. Rev. A 23, 2660–2663.

Pollack, G.L., Himm, J.F., 1982. Solubility of xenon in liquid *n*-alkanes: temperature dependence and thermodynamic functions. J. Chem. Phys. 77, 3221–3229.

Roche C.T., Strauss, M.G., Brenner, R., 1985. IEEE Trans. Nucl. Sci. NS-323 73–379.

Roth, M., 1987. Best density maps in low-resolution crystallography with contrast variation. Acta Crystallogr. A 43, 780–787.

Roth, M., 1991. Phasing at low resolution. In: Moras, D., Podjarny, A.D., Thierry, J.C. (Eds.), Crystallographic Computing, vol. 5. Oxford Univ. Press, New York, pp. 229–248.

Roth, M., Arnoux, B., Ducruix, A., Reiss-Husson, F., 1991. Structure of the detergent phase and protein–detergent interactions in crystals of the wild-type (strain Y) *Rhodobacter sphaeroides* photochemical reaction center. Biochemistry 30, 9403–9413.

Roth, M., Lewit-Bentley, A., Bentley, G.A., 1984. Scaling and phase-difference determination in solvent contrast variation experiments. J. Appl. Crystallogr. 17, 77–84.

Roth, M., Lewit-Bentley, A., Michel, H., Deisenhofer, J., Huber, R., Oesterhelt, D., 1989. Detergent structure in crystals of a bacterial photosynthetic reaction centre. Nature 340, 659–662.

Sauer, O., Roth, M., Schirmer, T., Rummel, G., Kratky, C., 2002. Low-resolution detergent tracing in protein crystals using xenon or krypton to enhance X-ray contrast. Acta Crystallogr. D 58, 60–69.

Snijder, H.J., Dijkstra, B.W., 2000. Bacterial phospholipase A, structure and function of an integral membrane phospholipase. Biochim. Biophys. Acta 1488, 91–101.

Snijder, H.J., Ubarretxena-Belandia, I., Blaauw, M., Kalk, K.H., Verheij, H.M., Egmond, M.R., Dekker, N., Dijkstra, B.W., 1999.

Structural evidence for dimerization-regulated activation of an integral membrane phospholipase. Nature 401, 717–721.

Timmins, P., Pebay-Peyroula, E., Welte, W., 1994. Detergent organisation in solutions and in crystals of membrane proteins. Biophys. Chem. 53, 27–36.

Timmins, P.A., Hauk, J., Wacker, T., Welte, W., 1991. The influence of heptane-1,2,3-triol on the size and shape of LDAO micelles. Implications for the crystallisation of membrane proteins. FEBS Lett. 280, 115–120.

Vandeputte-Rutten, L., Kramer, R.A., Kroon, J., Dekker, N., Egmond, M.R., Gros, P., 2001. Crystal structure of the outer membrane protease OmpT from *Escherichia coli* suggests a novel catalytic site. EMBO J. 20, 5033–5039.

Vogt, J., Schulz, G.E., 1999. The structure of the outer membrane protein OmpX from *Escherichia coli* reveals possible mechanisms of virulence. Structure 7, 1301–1309.

Weast, R.C., Astle, M.J. (Eds.), 1983. Handbook of Chemistry and Physics, vol. 1, 63rd ed.. CRC Press, Boca Raton, FL.